Title
Subnanometer-sized Pt/Sn alloy cluster catalysts for the dehydrogenation of linear alkanes

Journal
Physical Chemistry Chemical Physics, 15(47)

ISSN
0956-5000

Authors
Hauser, Andreas W
Gomes, Joseph
Bajdich, Michal
et al.

Publication Date
2013

DOI
10.1039/c3cp53796j

Peer reviewed

PCCP

RSC Publishing

PAPER

View Article Online
View Journal | View Issue

Cite this: *Phys. Chem. Chem. Phys.*, 2013, **15**, 20727

Subnanometer-sized Pt/Sn alloy cluster catalysts for the dehydrogenation of linear alkanes

Andreas W. Hauser,*[a] Joseph Gomes,[a] Michal Bajdich,[a] Martin Head-Gordon*[b] and Alexis T. Bell*[a]

Received 6th September 2013,
Accepted 21st October 2013

DOI: 10.1039/c3cp53796j

www.rsc.org/pccp

The reaction pathways for the dehydrogenation of ethane, propane, and butane, over Pt are analyzed using density functional theory (DFT). Pt nanoparticles are represented by a tetrahedral Pt_4 cluster. The objectives of this work were to establish which step is rate limiting and which one controls the selectivity for forming alkenes as opposed to causing further dehydrogenation of adsorbed alkenes to produce precursors responsible for catalyst deactivation due to coking. Further objectives of this work are to identify the role of adsorbed hydrogen, derived from H_2 fed together with the alkane, on the reaction pathway, and the role of replacing one of the four Pt atoms by a Sn atom. A comparison of Gibbs free energies shows that in all cases the rate-determining step is cleavage of a C–H bond upon alkane adsorption. The selectivity to alkene formation *versus* precursors to coking is dictated by the relative magnitudes of the activation energies for alkene desorption and dehydrogenation of the adsorbed alkene. The presence of an adsorbed H atom on the cluster facilitates alkene desorption relative to dehydrogenation of the adsorbed alkene. Substitution of a Sn atom in the cluster to produce a Pt_3Sn cluster leads to a downward shift of the potential energy surface for the reaction and causes an increase of the activity of the catalyst as suggested by recent experiments due to the lower net activation barrier for the rate limiting step. However, the introduction of Sn does not alter the relative activation barriers for gas-phase alkene formation *versus* loss of hydrogen from the adsorbed alkene, the process leading to the formation of coke precursors.

1. Introduction

Ethene, propene, and butene are building blocks for a wide array of commodity and specialty chemicals. While traditionally produced by the steam cracking of petroleum-derived naptha, the production of these light alkenes *via* thermal dehydrogenation of C2–C4 alkanes present in natural gas and other sources is an attractive alternative since it minimizes the formation of methane and coke as byproducts. Platinum, in the form of supported nanoparticles, is one of the most suitable catalysts for the thermal dehydrogenation of light alkanes. The high activity of Pt is a consequence of its high density of electronic states close to the Fermi level,[1–3] a characteristic that contributes to C–H bond activation.[4] However, unpromoted Pt catalysts suffer from two drawbacks – the first is low alkene selectivity and the second is rapid deactivation due to coking. Both of these characteristics are a consequence of alkene re-adsorption, which leads to further dehydrogenation and C–C bond breaking.[5,6]

A number of authors have shown that superior catalyst activity, selectivity, and stability can be achieved by alloying Pt with Sn and by adding hydrogen to the alkane feed.[5,7–11] Both aspects have been addressed in recent experiments of our group on the dehydrogenation of ethane over Pt_xSn_{100-x} clusters ($70 \leq x \leq 100$).[12] First, it has been observed that the presence of hydrogen suppresses the formation of coke and enhances the rate of alkane dehydrogenation, if the ratio of H_2 to alkane is below about 1.5. The mechanism behind this improvement is poorly understood. For higher H_2/alkane ratios the rate of alkene formation decreases due to its hydrogenation. Second, it has been shown that the addition of Sn promotes the catalytic activity and selectivity towards ethene *versus* the formation of methane and coke. In the past, these improvements have been attributed to both geometric as well as electronic effects.[13–19] Tin atoms on the surface of Pt clusters are known to frustrate the formation of larger active ensembles, which suppresses undesired C–C bond cleavage processes that lead to coke formation and deactivation.[9,20–27] Careful comparison

[a] *Department of Chemical and Biomolecular Engineering, University of California, Berkeley, CA 94720-1462, USA. E-mail: andreas.w.hauser@gmail.com, alexbell@uclink.berkeley.edu*

[b] *Department of Chemistry, University of California, Berkeley, CA 94720-1462, USA. E-mail: mhg@cchem.berkeley.edu*

of catalyst activities at varying residence times reveals an intrinsically higher activity of the alloy compared to pure Pt clusters,[12] indicating the presence of beneficial electronic effects as suggested by theoretical work on metal surfaces.[16,17] More recent computational studies on bulk catalysts predict PtSn surfaces to be less active but more selective: the presence of tin reduces the adsorption energies for propane on PtSn surfaces, but it also lowers the desorption barrier for propene, while it simultaneously increases the barrier for propene dehydrogenation.[28,29]

The aim of the present study was to obtain additional insights into the factors governing the energetics of C–H cleavage processes over Pt nanoparticles. To this end, we have carried out a computational study on a drastically reduced prototype of an active site, in order to focus on two issues: (1) the influence of hydrogen gas on the dehydrogenation of light alkanes and (2) the effects of partial replacement of Pt by Sn. Our model consists of four Pt metal atoms in tetrahedral geometry. This minimum system was chosen because it has a well defined geometry (in contrast to larger clusters with numerous isomers of almost identical energies), is representative of undercoordination occurring in small Pt-clusters, and is computationally accessible due to its simplicity. This makes it a highly suitable model for an analysis of electronic modifications without being biased by geometry effects. Another feature of our Pt_4 model is that the replacement of a single Pt atom by Sn leads to the correct stoichiometric ratio of a typical Pt–Sn alloy, allowing us a direct study of electronic effects on the reaction path. While the size of the cluster used in this work is smaller than that of Pt nanoparticles used in most experimental work (1–4 nm), there have been recent reports of alkane dehydrogenation on size-selected Pt clusters consisting of 8 to 10 atoms, stabilized on high-surface-area supports.[30] Experimental studies of unsupported clusters containing up to 24 Pt atoms have also been reported for the activation of methane.[31] Among the smallest clusters, particular attention has been paid to Pt tetramers and methane dehydrogenation.[32,33]

2. Computational methods

Platinum nanoparticles are represented by four atoms in a tetrahedral geometry with triplet spin multiplicity. Previous studies have shown this structure and spin state to be the most stable for Pt_4 isomers.[34–36] The activation of ethane, propane and butane on Pt_4 is investigated by means of density functional theory (DFT), using the B3LYP functional[37–40] together with the standard split-valence 6-31G** basis set[41] for H, C and O and the LANL2DZ basis set/effective core potential[42,43] for Pt and Sn atoms. Cartesian d functions are used in all calculations. Details of the SCF convergence and the geometry optimization thresholds are given elsewhere.[44] The lowest state of the singlet spin manifold shows a square-planar geometry, lying 0.28 eV above the tetrahedral triplet configuration. The lowest energy configuration for Pt_3Sn is also found to be tetrahedral, but has singlet multiplicity. All minima and intermediates are obtained in fully unrestrained geometry optimizations. Transition states are estimated with the freezing string method[45] and localized by an eigenvector-following approach[46] in Q-Chem.[47] Gibbs free energies are calculated within the harmonic oscillator approach at all relevant minima and transition states on the electronic potential energy surface, including zero-point energy corrections. All translational, rotational and vibrational degrees of freedom are taken into consideration. To benchmark the quality of our thermochemistry results for the chosen computational approach we calculate the reaction enthalpy at standard conditions for the dehydrogenation of propane and obtain a value of 22.7 kcal mol^{-1}, which is in reasonable agreement with the experimentally measured value of 20.1 kcal mol^{-1}.[48,49]

We note that the computational method and basis set size were chosen to allow for a rapid and efficient exploration of the potential energy surface of all alkanes considered here, but can only be expected to give qualitative results and useful indications of trends. Although the system size would in principle allow for larger basis sets and alternative approaches such as RI-MP2, any gain in computational accuracy has to be measured against the severe simplifications which are intrinsic in the model of a free-standing Pt_4 cluster: energy shifts due to distortions of the catalyst geometry and due to changes in the electronic structure, which inevitably occur as soon as the clusters are deposited on any type of substrate, and the uncertainties introduced by particle size distributions are at least of the same order of magnitude as errors introduced by a lack of correlation energy or a finite basis set. A series of benchmark calculations presented in ref. 30 indicates minor deviations of about 0.1 eV in electronic energies with respect to the effects of cluster size and nanoparticle support.

3. Results and discussion

The reaction path and the cluster geometries for the dehydrogenation of propane are given in Fig. 1. The corresponding energies are summarized in Table 1 and compared to energies for ethane and butane activation. The general outline of the reaction path is the same for all three molecules: after physisorption[50] to the cluster in step A1, the alkane undergoes C–H bond cleavage *via* the transition state A2, in which one hydrogen atom is taken from the beta carbon atom. This leads to an intermediate state A3 with an H atom and a 2-propyl group attached to the same corner of the cluster. The hydrogen atom then migrates *via* the transition state A4 to a different corner of the cluster, forming the intermediate A5. Removal of a second hydrogen atom occurs, as shown in Fig. 1, *via* transition state A6, which involves the cleavage of a C–H bond associated with the alpha carbon of the 2-propyl group. While the energies of the first five steps of the propane dehydrogenation process agree with those reported previously to within about 0.1 kcal mol^{-1},[30] our calculations indicated a different, more direct route for the cleavage of the second hydrogen atom *via* transition state A6. The barrier for C–H bond breaking is slightly lower for a hydrogen migration along the same edge of the tetrahedron than it is along other edges. We obtain an intermediate state A7

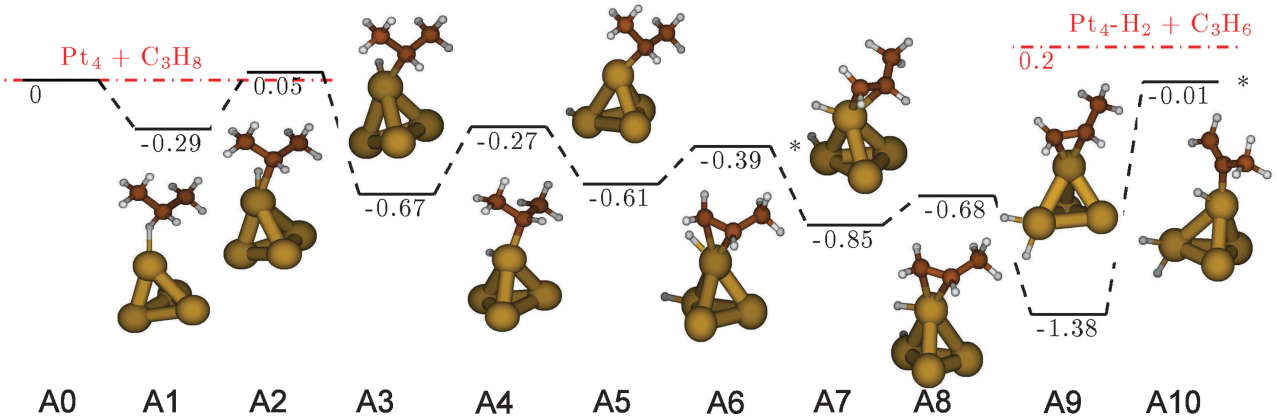

Fig. 1 B3LYP energies and geometries for the dehydrogenation reaction of propane on Pt_4 (states labeled as A). Energies are plotted in eV units, relative to the energy of pristine Pt_4 and a free propane molecule. Transition states that correspond to the cleavage of a C–H bond are marked with stars. The energies for desorbed gas molecules of propane and propene are given as red dash-dotted lines.

Table 1 Steps of the dehydrogenation reaction for alkanes attached to Pt_4, given the example of propane. The corresponding geometries can be found in Fig. 1

Structure	Label	ΔE^a (eV)	E (Hartree)
Pt_4, C_3H_8	A0	0.00	−595.774718
Pt_4–C_3H_8	A1	−0.29	−595.785289
C–H breaking	A2	0.05	−595.772939
Pt_4–H–C_3H_7	A3	−0.67	−595.799286
H migration	A4	−0.27	−595.784810
Pt_4–H–C_3H_7	A5	−0.61	−595.797121
C–H breaking	A6	−0.39	−595.788958
Pt_4–H–H–C_3H_6	A7	−0.85	−595.806040
H migration	A8	−0.68	−595.799666
Pt_4–H–H–C_3H_6	A9	−1.38	−595.825261
C–H breaking	A10	−0.01	−595.775045

[a] Relative to the energy of pristine Pt_4 and a desorbed propane molecule (A0).

with one H atom and the remaining alkene coordinated to the same corner and the previous H atom at a different corner. After another hydrogen migration *via* state A8, the minimum energy geometry A9 is reached in which both hydrogen atoms are attached to the same corner of the cluster. Removal of a third hydrogen atom *via* the transition state A10 competes with the desorption of a propene molecule. The desorption energy for propene is given as red dashed line in Fig. 1, and is only 0.19 eV above transition state A10 which must be overcome for further dehydrogenation. The desorption of a C_3H_7 propyl radical is not shown since this process requires a significantly higher energy input of about 2 eV.

As can be seen from Fig. 1 the first C–H cleavage at A2 constitutes the rate-determining step. This process has a barrier height of only 0.05 eV, which is significantly lower than the barrier (0.70 eV) calculated for propane dehydrogenation on bulk Pt (111).[28] This indicates a strong dependence of the activity on the local geometry of the active site. Our propane adsorption energy of −0.29 eV, on the other hand, is close to the experimental value measured for Pt (111), which lies between −0.35 and −0.44 eV.[51–53] A slightly weaker physisorption on the cluster is plausible given the reduced number of Pt neighbors in the tetrahedral model for attractive van der Waals interaction.

Having identified the potential energy changes occurring during the dehydrogenation, we next determine changes in Gibbs free energies. The information needed to calculate the zero-point energy correction, the entropy and enthalpy, was obtained from frequency calculations at the relevant geometries within the harmonic oscillator approach. Steps related to hydrogen migration on the metal cluster yield no new chemical insights and were skipped for brevity. Repeating this procedure for ethane and butane we obtain a set of condensed reaction pathways shown in Fig. 2. The first row in each plot refers directly to the relative (and purely electronic) *ab initio* energy in kcal mol^{-1} as obtained from density functional theory (T = 0 K, p = 0 bar), while the second contains the Gibbs free energies at 400 °C and 1 bar, corresponding to the low-temperature side of the typical experimental range for the dehydrogenation of alkanes over platinum catalysts.[7,30,54–56] It can be seen that the thermodynamic corrections raise the barriers for the C–H cleavage steps. At higher temperature, all three steps of hydrogen removal (A2, A6 and A10) lie above the Gibbs free energy for gas-phase propane, but the first C–H bond breaking remains the rate-limiting step. The gain in entropy for desorption at higher temperature leads to an inversion of the ordering at A10: the desorption of the alkenes becomes more favorable than the third C–H cleavage step, which explains the desired and experimentally observed high selectivity towards alkene formation.

3.1. The influence of hydrogen adsorption

We next consider the influence of adsorbed hydrogen on the reaction pathway. This effort is motivated by recent experimental work of our group, which show a maximum ethene formation rate at a hydrogen to ethane ratio of 3 : 2 in the gas feed.[12] For higher ratios of hydrogen gas the conversion rate drops and converges to the equilibrium value for the reaction $C_2H_6 \rightleftharpoons C_2H_4 + H_2$ dictated by thermodynamics. The presence of some hydrogen is known to be advantageous,[5] and has been mainly attributed to a reduction in the rate of coke formation.

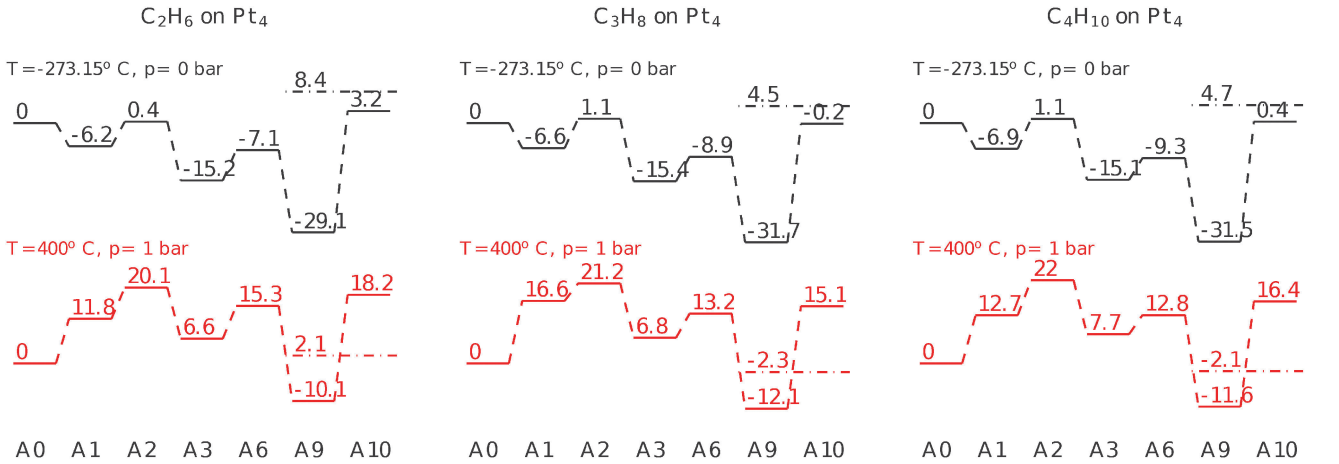

Fig. 2 Gibbs free energies for the dehydrogenation reaction of ethane, propane and butane (from left to right) attached to Pt_4, at zero Kelvin and at experimental conditions. Energy units are kcal mol^{-1}. Each transition state corresponds to the breaking of a C–H bond. Transition states of hydrogen migration on Pt_4 have been omitted for clarity. Energies for a desorbed alkene molecule are given as dash-dotted lines. At higher temperature the desorption of the alkenes is more likely than a further dehydrogenation (step A10) due to the gain in entropy.

However, even at very low residence times, where the re-adsorption of alkenes is minimized, co-feeding hydrogen gas promotes the activity of the catalyst. This suggests a beneficial electronic effect related to a partial coverage of the catalyst with hydrogen.

As a first step in analyzing the effects of hydrogen coverage on the dehydrogenation of alkanes we determined the thermodynamics of hydrogen adsorption on Pt_4 clusters as a function of the H_2 pressure and the temperature. This is most easily done by the construction of a (p,T)-phase diagram for Pt_4H_n on the basis of the potential ω which we define as

$$\omega(T,\mu_H,n) = \Delta E_{F,corr} - T{\cdot}s_{Pt_4H_n} - \mu_H{\cdot}n. \qquad (1)$$

Assuming a constant number N of Pt_4 clusters but arbitrary amounts of hydrogen molecules in the system, we write $\omega(T,\mu_H,n)$, the grand potential Ω divided by N, as a function of the temperature T, the chemical potential of hydrogen μ_H, and the number of adsorbed hydrogen atoms n. The Pt_4 clusters are treated as immobilized on a surface which is coupled to a heat bath of temperature T and an infinite reservoir of H_2 gas at pressure p. Given this idealized setup, $\omega(T,\mu_H,n)$ will be a minimum at thermodynamic equilibrium. With a pressure dependence entering *via* $\mu_H(p,T)$ we can now predict which value of n minimizes ω for a specified temperature and H_2 pressure by simply evaluating the right hand side of eqn (1):

The first term in eqn (1), $\Delta E_{F,corr}$, corresponds to the zero-point-energy corrected formation energy of Pt_4H_n defined as

$$\Delta E_{F,corr} = E_{Pt_4H_n} - E_{Pt_4} - n/2{\cdot}E_{H_2} + E_{corr}. \qquad (2)$$

$E_{Pt_4H_n}$ and E_{Pt_4} denote the DFT energies of the hydrogen-covered and pure cluster, respectively, and E_{H_2} is the DFT energy of molecular hydrogen. The temperature-independent zero-point energy corrections have been absorbed into the term E_{corr}. The uncorrected formation energies obtained with the B3LYP functional are listed in Table 2 and plotted in Fig. 3a. They show an almost linear dependence on the particle number, indicating a stepwise loading of the cluster without hydrogen interaction effects.

Table 2 B3LYP formation energies and spin multiplicities m of Pt_4H_n according to eqn (2) (without zero-point energy correction)

Cluster	m	$\Delta E_{F,uncorr}$ (eV)	Abs. energy (Hartree)
Pt_4	3	0.00	−476.619361
Pt_4H	4	−0.78	−477.237247
Pt_4H_2	3	−1.44	−477.850980
Pt_4H_3	4	−1.72	−478.450520
Pt_4H_4	3	−2.32	−479.061872
Pt_4H_5	2	−2.98	−479.675227
Pt_4H_6	1	−3.35	−480.278216
Pt_4H_7	2	−3.97	−480.890242
Pt_4H_8	1	−4.73	−481.507191

The second term on the right hand side of eqn (1) corrects the energy with respect to the entropy $s_{Pt_4H_n}$ of the cluster. Assuming the platinum clusters to be immobile only vibrational motion and electronic degrees of freedom can contribute to the cluster entropy. Vibrational entropies are taken from the thermochemistry output of Q-Chem for temperatures from 0 to 1000 °C, and are based on the harmonic oscillator approximation. The electronic contribution to entropy is calculated from the spin multiplicities m in Table 2 *via* the formula $s_{elec} = R\ln(m)$. Following the estimation of ref. 57 we neglect minimal contributions from electronically excited states.

The third and last term on the right side of eqn (1) is the chemical potential μ_H of hydrogen multiplied by the number n of adsorbates. This last term needs special care since it introduces the pressure dependence and is of the same magnitude as $\Delta E_{F,corr}$. For the estimation of μ_H we follow the approach used by previous authors in studies of cluster oxidation, and write the chemical potential of molecular hydrogen as[57–59]

$$\mu_{H_2} = \Delta h_{H_2}(p_0,T) - T\cdot s_{H_2}(p_0,T) + RT\ln\left(\frac{p}{p_0}\right). \qquad (3)$$

In this expression the pressure enters through the ratio p/p_0, with the reference hydrogen pressure p_0 set to 1 bar.

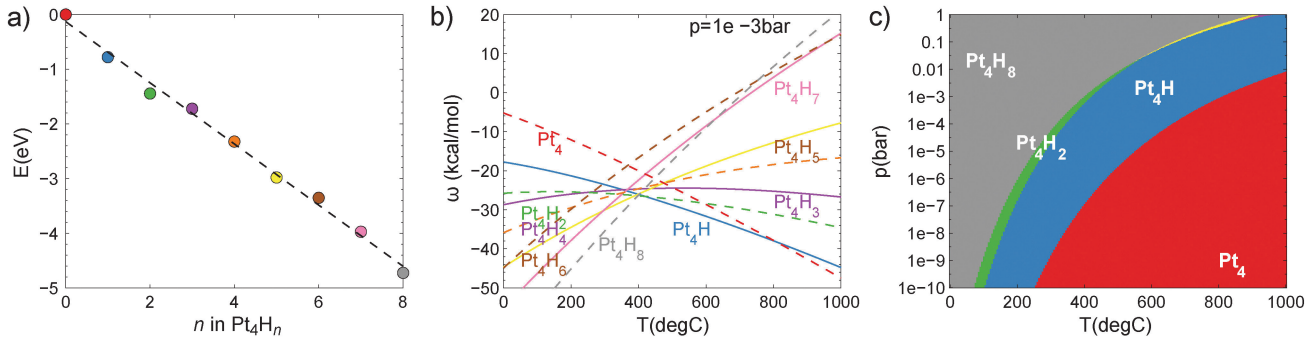

Fig. 3 (a) B3LYP formation energies (without zero-point energy corrections) of Pt_4H_n as a function of the hydrogen number n. The almost linear dependence is due to the marginal interaction of H atoms at different adsorption sites and the negligible influence on the cluster geometry. (b) The grand potential per platinum cluster, ω, as a function of the temperature at a pressure of 10^{-3} bar. Odd numbers of H atoms are plotted as dashed lines. The predicted phases can be retrieved from the convex hull of the lowest energy curves. At the given pressure one finds relevant phases with 8, 2, 1 and 0 hydrogen atoms attached. (c) Pt_4H_n phase diagram as a function of pressure and temperature. The single adsorption of hydrogen turns out to be a separating phase between full and zero coverage. The Pt_4H_2 phase occurs for sufficiently low pressures in a very narrow temperature range. The color coding is consistent in all three pictures.

The change of enthalpy is given by $\Delta h_{H_2} = h(p_0,T) - h(p_0,T = 0\ \mathrm{K})$. For maximum accuracy we take the values for h_{H_2} and s_{H_2} from the NIST database.[60] Assuming a chemical equilibrium in the reaction

$$n/2{\cdot}H_2(g) + Pt_4 \rightleftharpoons P_4H_n \qquad (4)$$

the chemical potential for hydrogen μ_H is equal to $\mu_{H_2}/2$.

Having defined all terms of eqn (1) we can calculate $\omega(p,T,n)$ for the experimentally relevant range of T = 0 to 1000 °C and p = 1 to 10^{-10} bar and determine the phase of lowest energy for each variable pair (p,T). The resulting phase diagram is given in Fig. 3c. The temperature dependence of ω is illustrated in Fig. 3b for a pressure of 10^{-3} bar. The position of the phase transitions for this particular pressure can be derived from the convex minimum-energy hull of the Pt_4H_n curves. Surprisingly, only four phases are to be expected in the given range, with a notably sharp transition from a single-atom coverage to an almost complete saturation of the tetrahedral model system. The Pt_4H phase is stable over a wide range of pressure and temperature. Before discussing the consequence of this result in the context of alkane activation we give a brief estimation of the uncertainty which is intrinsic to this approximate bottom-up approach based on electronic structure theory.

The largest uncertainty is introduced by the formation energies obtained from density functional theory. Benchmark calculations with different functionals indicate slight deviations in the range of a few tenths of eV, translating into a noticeable shift of phase transitions in Fig. 3b and c, but do not lead to qualitative changes in the overall phase diagram. Inaccuracies due to the simplified description of entropy, assuming the same vibrational modes for surface-mounted clusters as for gas phase clusters, and errors due to the harmonic approximation of frequencies, are small compared to the uncertainties in the electronic energy.

Having identified the most probable phases of Pt_4H_n we can now analyze the impact of hydrogen coverage on the dehydrogenation process. Obviously, a total coverage with hydrogen is undesirable as this favors the recombination of alkenes to alkanes and deactivates the catalyst by occupying the active sites. Hence, the only reasonable phase in our model system is Pt_4H, which also is the preferred phase at dehydrogenation temperatures above 600 °C for a hydrogen partial pressure below 0.1 bar. To investigate the influence of hydrogen on the reaction pathway for dehydrogenation we put one H atom at one of the corners of the Pt_4 cluster and recalculated the Gibbs free energies for propane dehydrogenation. Note that there are numerous intermediates and transition states of similar energy due to the mobility of hydrogen on the cluster. In a trial and error approach we tried to identify the geometries that yield the lowest energies. To analyze a trend towards higher hydrogen coverage we repeated this procedure also for the less likely Pt_4–H_2 phase. Fig. 4 compares the reaction pathways for Pt_4–H and Pt_4–H_2 with that for Pt_4. We find that the presence of one or two hydrogen atoms on the cluster has little effect on the adsorption of alkanes, but raises the Gibbs free energies of the transition states for the three C–H cleavages. Interestingly, it raises the energy of the third and undesired cleavage step to far greater extent than it does for the first two steps. A marginal effect on the first two C–H cleavages combined with a significant shift of the third suggests that the addition of small amounts of hydrogen gas could improve the selectivity of the reaction towards the formation of alkenes. The difference between alkene desorption (dashed lines in Fig. 4) and the energy barrier needed to be overcome for continued dehydrogenation (the conversion of species A9 to A10) increased from 17 to 25 and 20 kcal mol^{-1} for Pt_4H and Pt_4H_2, respectively. Interestingly, the shifting effect is more pronounced for single H atom coverage than for two atoms (*i.e.* a full saturation of one corner of the tetrahedron).

3.2. Subnanometer alloy catalysts: Introducing Sn

We have examined the influence of Sn on the performance of Pt clusters on the dehydrogenation of ethane, propane and butane, by comparing the Gibbs free energy profiles of dehydrogenation occurring in Pt_4 and Pt_3Sn. Since the replacement of one Pt atom by Sn has a negligible influence on the tetrahedral

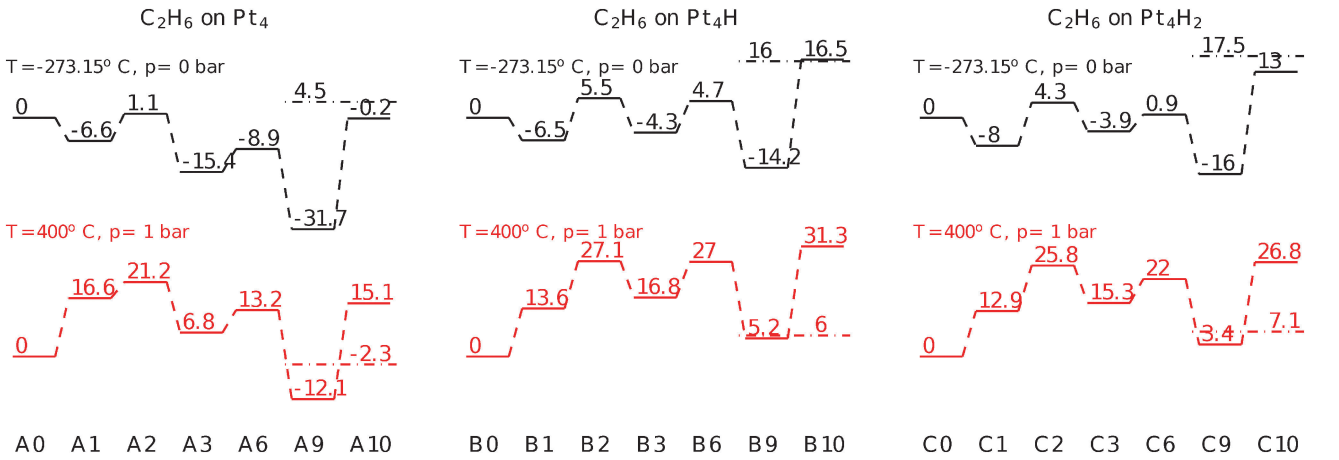

Fig. 4 Reaction pathways for the dehydrogenation of propane attached to Pt_4, Pt_4H and Pt_4H_2 (from left to right), at zero Kelvin and at experimental conditions. Energy units are kcal mol^{-1}. Each transition state corresponds to the breaking of a C–H bond. Transition states of hydrogen migration have been omitted for clarity. Energies for desorbed alkene molecules are given as dash-dotted lines.

structure, any difference in activity and selectivity between these models must be purely electronic. The corresponding reaction pathway diagrams are given in Fig. 5. Qualitatively, they are similar to those obtained for Pt_4 (see Fig. 2), but the atomic substitution shifts all of the steps to slightly lower energies. This effect becomes more pronounced the further the reaction proceeds, with shifts of about 1 kcal mol^{-1} for the physisorbed state A1, 3 kcal mol^{-1} for the intermediate A3 and about 5 kcal mol^{-1} for state A9, the trend being the same for all three alkanes. The barrier for the rate-determining step A2 is reduced by about 2 kcal mol^{-1} on average, suggesting that Sn addition may enhance the rate of alkane dehydrogenation. This beneficial effect comes at the cost of a reduced selectivity since the introduction of Sn also lowers the barrier for the undesired third C–H cleavage.

Interestingly, the effect of Sn on Pt_4 clusters is the exact opposite of what has been predicted for bulk alloy catalyst surfaces of Pt and Sn.[28] Alloying with the less reactive Sn increases the *d*-bandwidth of the material and shifts the center of the band to lower energies. A consequence of the reduced density at the Fermi level is an overall energy increase for all steps of the reaction pathway, making the alloy less active for propane dehydrogenation. On the other hand, this affects the third hydrogen removal in the same way and makes it less competitive with propene desorption, thereby improving the selectivity of the catalyst. This discrepancy between bulk Pt and our cluster model can be explained by a Mulliken charge analysis of Pt_4 and Pt_3Sn, which reveals that the uncharged Pt atoms in the tetrahedral Pt_4 become negatively charged $(-1/4e)$ upon replacing one of the Pt atoms with an electron-donating Sn atom $(+3/4e)$. The increased electron density at the active site lowers all energies of the reaction path, while the positively charged Sn atom becomes the avoided, inactive corner of the catalyst. Obviously, such a distinctive local effect cannot occur on a perfect, periodic surface of a bulk Pt/Sn alloy catalyst. What remains in the bulk is an overall, slight reduction of

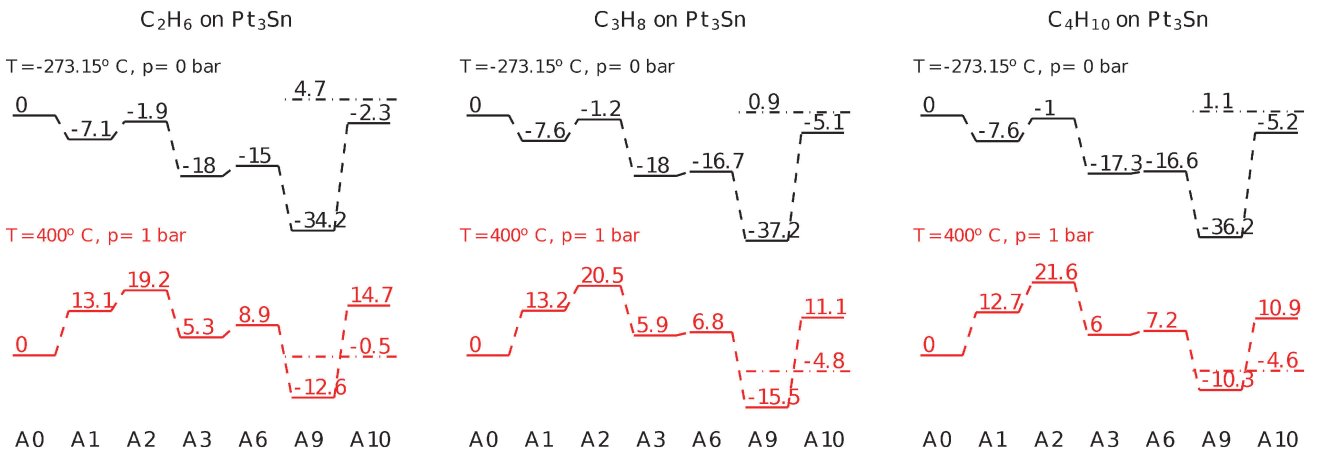

Fig. 5 Gibbs free energies for the dehydrogenation reaction of ethane, propane and butane (from left to right) at zero Kelvin and at experimental conditions, attached to Pt_3Sn. Energy units are kcal mol^{-1}. Each transition state corresponds to the breaking of a C–H bond. Transition states of hydrogen migration have been omitted for clarity. Energies for a desorbed alkene molecule are given as dash-dotted lines.

electron density at the Fermi level, which shifts the reaction path towards higher energies.

To summarize, the comparison between Pt_4 and Pt_3Sn indicates that in the case of finite nanoparticles a transfer of negative charge from the electron-donating Sn atom to the active site of the cluster is responsible for a higher activity but reduced selectivity of the catalyst. For propane the energetic difference between further dehydrogenation and alkene desorption at 400 °C is shrinking from 17.4 (Pt_4) to 15.9 (Pt_3Sn) kcal mol^{-1}, indicating only a minimal impact on the preference towards desorption.

4. Conclusion

A theoretical analysis of the elementary processes involved in the dehydrogenation of ethane, propane, and butane was carried out with the aim of establishing what factors influence the formation of gas-phase alkenes *versus* further loss of hydrogen from adsorbed alkene leading to formation of coke precursors. The calculations were carried out using a tetrahedral Pt_4 cluster to represent small Pt nanoparticles dispersed on a support. Using this model we were also able to explore the impact of two substantial modifications on catalyst performance: (a) the partial coverage of the catalyst with H atoms derived from the adsorption of H_2 introduced into the feed and (b) the replacement of a single Pt atom by Sn to model the effect of alloying with Sn on the nanoscale. Both objectives are triggered by recent experimental discoveries of positive effects on the selectivity and activity of the alkane-to-alkene conversion of H_2 addition to the feed and alloying of Pt with Sn. We draw the following conclusions:

(1) Our studies show that for all alkanes investigated (ethane, propane, butane) and for both Pt_4 and Pt_3Sn the cleavage of the first C–H bond is the rate-determining step. The same conclusion is reached when one or two atoms of H are adsorbed on a Pt_4 cluster (*i.e.*, Pt_4H, Pt_4H_2).

(2) The remarkable selectivity towards alkene production is explained by the higher barriers for the cleavage of the third hydrogen atom in combination with low alkene binding energies which decrease even further with increasing temperature. At room temperature and above the desorption of the product alkene is more likely than further C–H bond cleavage.

(3) The co-feeding of hydrogen, to reduce coking, can be simulated with the Pt_4 model. The cluster is stable upon hydrogen adsorption, enabling investigation of the influence of adsorbed H atoms on the reaction pathway without effects induced by changes in cluster geometry. A phase diagram based on thermodynamic data derived from DFT calculations predicts one stable phase, Pt_4H, for H_2 partial pressures and temperatures typical of those used in experimental studies (below 0.1 bar and above 600 °C). This phase shows an improved selectivity towards alkene production: the third C–H cleavage step is shifted to higher energy, making it even less competitive to the preferred alkene desorption. This comes at the cost of a slightly reduced activity as the presence of hydrogen shifts all transition states to some extent, including the rate-determining first C–H cleavage step.

(4) Replacement of a single Pt atom by Sn does not change the overall geometry of the model but has strong effects on the reaction pathway. Our results show substitution of a Pt atom by an Sn atom in Pt_4 to produce a tetrahedral Pt_3Sn cluster adds negative charge to the active Pt site, causing a downward shift in the potential energy surface for the reaction. The net result of this effect is to increase the activity of the catalyst due to the lower net activation barrier for the rate limiting step. However, the introduction of Sn does not alter the relative activation barriers for gas-phase alkene formation *versus* loss of hydrogen from the adsorbed alkene, the process leading to the formation of coke precursors.

Acknowledgements

This research was supported by the XC^2 program funded by BP. Calculations were performed on a cluster provided by the UC Berkeley College of Chemistry through the National Science Foundation (NSF) (Grant CHE-1048789).

References

1 R. V. Chepulskii and S. Curtarolo, *ACS Nano*, 2011, **5**, 247–254.
2 J. K. Norskov and F. Abild-Pedersen, *Nature*, 2009, **461**, 1223–1225.
3 J. K. Norskov, T. Bligaard, J. Rossmeisl and C. H. Christensen, *Nat. Chem.*, 2009, **1**, 37–46.
4 A. T. Bell, *Science*, 2003, **299**, 1688–1691.
5 V. Galvita, G. Siddiqi, P. Sun and A. T. Bell, *J. Catal.*, 2010, **271**, 209–219.
6 A. Virnovskaia, E. Rytter and U. Olsbye, *Ind. Eng. Chem. Res.*, 2008, **47**, 7167–7177.
7 O. A. Bariås, A. Holmen and E. A. Blekkan, *J. Catal.*, 1996, **158**, 1–12.
8 F. Delbecq and P. Sautet, *J. Catal.*, 2003, **220**, 115–126.
9 M. S. Kumar, D. Chen, A. Holmen and J. C. Walmsley, *Catal. Today*, 2009, **142**, 17–23.
10 S. Slimane Laref, F. Delbecq and D. Loffreda, *J. Catal.*, 2009, **265**, 35–42.
11 F. Vigné, J. Haubrich, D. Loffreda, P. Sautet and F. Delbecq, *J. Catal.*, 2010, **275**, 129–139.
12 J. Wu, Z. Peng and A. T. Bell, *J. Catal.*, in review.
13 J. Shen, J. M. Hill, R. M. Watwe, B. E. Spiewak and J. A. Dumesic, *J. Phys. Chem. B*, 1999, **103**, 3923–3934.
14 R. M. Watwe, R. D. Cortright, M. Mavrikakis, J. K. Norskov and J. A. Dumesic, *J. Chem. Phys.*, 2001, **114**, 4663–4668.
15 E. Janin, H. von Schenck, S. Ringler, J. Weissenrieder, T. Åkermark and M. Göthelid, *J. Catal.*, 2003, **215**, 245–253.
16 R. Alcala, J. W. Shabaker, G. W. Huber, M. A. Sanchez-Castillo and J. A. Dumesic, *J. Phys. Chem. B*, 2005, **109**, 2074–2085.
17 J. Essen, J. Haubrich, C. Becker and K. Wandelt, *Surf. Sci.*, 2007, **601**, 3472–3480.

18 A. Virnovskaia, S. Morandi, E. Rytter, G. Ghiotti and U. Olsbye, *J. Phys. Chem. C*, 2007, **111**, 14732–14742.
19 A. Virnovskaia, S. Jørgensen, J. Hafizovic, O. Prytz, E. Kleimenov, M. Hävecker, H. Bluhm, A. Knop-Gericke, R. Schlögl and U. Olsbye, *Surf. Sci.*, 2007, **601**, 30–43.
20 R. Rennard and J. Freel, *J. Catal.*, 1986, **98**, 235–244.
21 Y.-L. Tsai and B. E. Koel, *J. Phys. Chem. B*, 1997, **101**, 2895–2906.
22 G. J. Siri, J. M. Ramallo-Lpez, M. L. Casella, J. L. Fierro, F. G. Requejo and O. A. Ferretti, *Appl. Catal., A*, 2005, **278**, 239–249.
23 P. Biloen, J. Helle and W. Sachtler, *J. Catal.*, 1979, **58**, 95–107.
24 F. Ribeiro, A. Bonivardi, C. Kim and G. Somorjai, *J. Catal.*, 1994, **150**, 186–198.
25 M. P. Lobera, C. Téllez, J. Herguido and M. Menéndez, *Appl. Catal., A*, 2008, **349**, 156–164.
26 Z. Nawaz, X. Tang, Q. Zhang, D. Wang and W. Fei, *Catal. Commun.*, 2009, **10**, 1925–1930.
27 S. Pisduangdaw, J. Panpranot, C. Methastidsook, C. Chaisuk, K. Faungnawakij, P. Praserthdam and O. Mekasuwandumrong, *Appl. Catal., A*, 2009, **370**, 1–6.
28 M.-L. Yang, Y.-A. Zhu, X.-G. Zhou, Z.-J. Sui and D. Chen, *ACS Catal.*, 2012, **2**, 1247–1258.
29 L. Nykänen and K. Honkala, *J. Phys. Chem. C*, 2011, **115**, 9578–9586.
30 S. Vajda, M. J. Pellin, J. P. Greeley, C. L. Marshall, L. A. Curtiss, G. A. Ballentine, J. W. Elam, S. Catillon-Mucherie, P. C. Redfern, F. Mehmood and P. Zapol, *Nat. Mater.*, 2009, **8**, 213–216.
31 D. J. Trevor, D. M. Cox and A. Kaldor, *J. Am. Chem. Soc.*, 1990, **112**, 3742–3749.
32 U. Achatz, C. Berg, S. Joos, B. S. Fox, M. K. Beyer, G. Niedner-Schatteburg and V. E. Bondybey, *Chem. Phys. Lett.*, 2000, **320**, 53–58.
33 C. Adlhart and E. Uggerud, *Chem. Commun.*, 2006, 2581–2582.
34 L. Xiao and L. Wang, *J. Phys. Chem. A*, 2004, **108**, 8605–8614.
35 L. Xiao and L. Wang, *J. Phys. Chem. B*, 2007, **111**, 1657–1663.
36 J. Kua and W. A. Goddard, *J. Phys. Chem. B*, 1998, **102**, 9481–9491.
37 A. D. Becke, *Phys. Rev. A: At., Mol., Opt. Phys.*, 1988, **38**, 3098–3100.
38 C. Lee, W. Yang and R. G. Parr, *Phys. Rev. B: Condens. Matter Mater. Phys.*, 1988, **37**, 785–789.
39 A. D. Becke, *J. Chem. Phys.*, 1993, **98**, 1372–1377.
40 A. D. Becke, *J. Chem. Phys.*, 1993, **98**, 5648–5652.
41 P. Hariharan and J. Pople, *Theor. Chim. Acta*, 1973, **28**, 213–222.
42 P. J. Hay and W. R. Wadt, *J. Chem. Phys.*, 1985, **82**, 270–283.
43 W. R. Wadt and P. J. Hay, *J. Chem. Phys.*, 1985, **82**, 284–298.
44 The SCF convergence in all optimizations is set to 10^{-9} Hartree, for the DFT grid size we choose 75 radial and 302 Lebedev angular points. The convergence thresholds for the maximum gradient component and for the energy difference of successive optimization steps are set to 3×10^{-5} and 4×10^{-7} Hartree, respectively.
45 A. Behn, P. M. Zimmerman, A. T. Bell and M. Head-Gordon, *J. Chem. Phys.*, 2011, **135**, 224108.
46 J. Baker, *J. Comput. Chem.*, 1986, **7**, 385–395.
47 Y. Shao, L. F. Molnar, Y. Jung, J. Kussmann, C. Ochsenfeld, S. T. Brown, A. T. Gilbert, L. V. Slipchenko, S. V. Levchenko, D. P. O'Neill, R. A. DiStasio Jr, R. C. Lochan, T. Wang, G. J. Beran, N. A. Besley, J. M. Herbert, C. Yeh Lin, T. Van Voorhis, S. Hung Chien, A. Sodt, R. P. Steele, V. A. Rassolov, P. E. Maslen, P. P. Korambath, R. D. Adamson, B. Austin, J. Baker, E. F. C. Byrd, H. Dachsel, R. J. Doerksen, A. Dreuw, B. D. Dunietz, A. D. Dutoi, T. R. Furlani, S. R. Gwaltney, A. Heyden, S. Hirata, C.-P. Hsu, G. Kedziora, R. Z. Khalliulin, P. Klunzinger, A. M. Lee, M. S. Lee, W. Liang, I. Lotan, N. Nair, B. Peters, E. I. Proynov, P. A. Pieniazek, Y. Min Rhee, J. Ritchie, E. Rosta, C. David Sherrill, A. C. Simmonett, J. E. Subotnik, H. Lee Woodcock III, W. Zhang, A. T. Bell, A. K. Chakraborty, D. M. Chipman, F. J. Keil, A. Warshel, W. J. Hehre, H. F. Schaefer III, J. Kong, A. I. Krylov, P. M. W. Gill and M. Head-Gordon, *Phys. Chem. Chem. Phys.*, 2006, **8**, 3172–3191.
48 S. Furuyama, D. M. Golden and S. W. Benson, *J. Chem. Thermodyn.*, 1969, **1**, 363–375.
49 D. A. Pittam and G. Pilcher, *J. Chem. Soc., Faraday Trans. 1*, 1972, **68**, 2224–2229.
50 Several adsorption scenarios are possible, but differ only minimally in energy. For propane, the physisorption of a terminal C group is less than 0.1 kcal mol^{-1} lower in energy than the adsorption of the center C group. However, following ref. 30, C–H bond breaking at a central carbon is preferred over a terminal carbon, making this reaction pathway the preferred one.
51 M. McMaster, C. Arumainayagam and R. Madix, *Chem. Phys.*, 1993, **177**, 461–472.
52 C.-L. Kao and R. J. Madix, *Surf. Sci.*, 2004, **557**, 215–230.
53 G. W. Cushing, J. K. Navin, S. B. Donald, L. Valadez, V. Johánek and I. Harrison, *J. Phys. Chem. C*, 2010, **114**, 17222–17232.
54 C. Yu, Q. Ge, H. Xu and W. Li, *Appl. Catal., A*, 2006, **315**, 58–67.
55 P. L. D. Cola, R. Gläser and J. Weitkamp, *Appl. Catal., A*, 2006, **306**, 85–97.
56 T. Waku, J. A. Biscardi and E. Iglesia, *Chem. Commun.*, 2003, 1764–1765.
57 Y. Xu, W. A. Shelton and W. F. Schneider, *J. Phys. Chem. B*, 2006, **110**, 16591–16599.
58 M. V. Bollinger, K. W. Jacobsen and J. K. Nørskov, *Phys. Rev. B: Condens. Matter Mater. Phys.*, 2003, **67**, 085410.
59 K. A. Persson, B. Waldwick, P. Lazic and G. Ceder, *Phys. Rev. B: Condens. Matter Mater. Phys.*, 2012, **85**, 235438.
60 M. W. Chase Jr., C. A. Davies, J. R. Downey Jr., D. J. Frurip, R. A. McDonald and A. N. Syverud, *NIST Standard Reference Database 13, NIST JANAF THERMOCHEMICAL TABLES 1985, Version 1.0, Standard Reference Data Program*, National Institute of Standards and Technology, Gaithersburg, MD 20899, http://kinetics.nist.gov/janaf/janbanr.html (accessed March 2013).

